Nonlinear Kinetic Parameter Identification through Map Inversion

Neil Shenvi, J. M. Geremia, and Herschel Rabitz*

Department of Chemistry, Princeton University, Princeton, New Jersey 08544

Received: July 31, 2002

A nonlinear method for parameter identification in kinetic systems is presented. Parameter identification is achieved through the use of HDMR (high-dimensional model representation), which can reduce greatly the computational cost of high-dimensional function inversion. The technique is demonstrated in simulations to extract rate constants from concentration data in a linear kinetic system, the reaction of H_2 with Br_2, and the oxidation of formaldehyde. The results of inversion for the latter case are compared with a previously published linear inversion procedure. The new algorithm shows excellent performance in identifying the full distribution of rate constants consitent with the data. The speed and accuracy of the HDMR permits full inversion of all relevant model parameters without the introduction of hidden biases from prior assumptions on the quality of the model parameters.

I. Introduction

Kinetic experiments are routinely performed to determine values for the rate constants of chemical reactions.[1−5] The reaction dynamics of such systems can often be modeled by a set of ordinary differential equations. Models of this type depend on many parameters, such as the rate constants, the initial concentrations, and the initial temperature. Some of these parameters can be estimated or may be measured directly. For instance, the initial concentrations of the species are usually known to some degree of accuracy. Similarly, a subset of the rate constants may be assigned values previously reported in the literature. The remaining unknown parameters must be determined by ensuring that the reaction model is consistent with the experimental data.[6]

The inversion problem of determining the unknown parameters is generally nonlinear even if the kinetic mechanism is linear (i.e., first-order). Thus, an analytic solution to the inverse problem frequently does not exist, and a nonlinear inversion technique must be used to find a set of parameters that best models the experimental data. The most common method of nonlinear kinetic parameter inversion involves model optimization using the conjugate gradient algorithm, or a variation thereof, which finds a locally optimal solution through a series of line minimizations.[7,8]

The gradient descent method and other nonlinear fitting methods, such as simulated annealing or genetic algorithms,[9] face several formidable obstacles when applied to chemical kinetic inversion. First, all nonlinear optimization routines rely on the repeated evaluation of the reaction model. In the case of chemical kinetics, this evaluation involves the integration of large systems of differential equations, which can be resource intensive and numerically difficult. Because an optimization can require thousands or even millions of model evaluations, the resources required for the inversion process can be prohibitive. Second, the volume of the searchable parameter space grows exponentially with the number of unknown parameters because each of the parameters can be varied independently. As a consequence, the number of trial parameters that must be sampled to obtain a good quality inversion can quickly become unmanageable, an obstacle referred to as the "curse of dimensionality".[10]

Third, chemical kinetics problems are often ill-posed in the sense that there can be multiple solutions that are consistent with the experimental data.[11,12] Because the distributions of the recovered parameter values are desired, it is insufficient to find only one solution. Instead, the parameter space must be thoroughly explored to ensure that all solutions consistent with the experimental data have been identified. A related issue is the estimation of errors in the parameters extracted from the nonlinear kinetic models. Monte Carlo methods have been proven effective in nonlinear error propagation, but they rely on large numbers of repeated model evaluations to produce meaningful statistics.[13,14]

The difficulties of high-dimensional chemical kinetic inversion can be palliated by replacing explicit evaluations of the kinetics for trial values of the rate constants with a *map* of the kinetics. A useful map function has the following characteristics:[10]

a. It approximates the actual reaction model to a high degree of accuracy.

b. It is easy to construct despite high-dimensionality.

c. It can be evaluated efficiently.

Such a map function can be used in place of the actual reaction model. Provided that the map function is sufficiently accurate, the optimal solutions obtained by inverting the map function will accurately approximate the solutions that would have been obtained by inverting the original reaction model. The increased efficiency of map evaluation relative to model evaluation permits a thorough sampling of the parameter space without requiring excessive resources. Thus, the full distribution of parameters consistent with the data can be determined.

In this paper, we have used map functions generated by the HDMR (high-dimensional model representation) algorithm, a general mapping technique that has been used successfully in a variety of problems.[10,15,16] The evaluation of HDMR maps requires only low-dimensional interpolation, making map evaluation very fast. In addition, the overhead associated with map construction is minimal because HDMR uses a relatively small set of representative kinetic models to learn the system's input−output relationship. The accuracy of the HDMR maps compared to the reaction model is problem dependent, but it was found

10.1021/jp021762e CCC: $22.00
Published on Web 12/04/2002

that HDMR maps were sufficiently accurate for all of the systems simulated here.

The contents of this paper are organized as follows: Section II describes the mathematical basis of HDMR and the implementation of the inversion algorithm. Section III discusses the results of the application of the algorithm to three kinetic systems. Conclusions are presented in section IV.

II. Technique

Nonlinear data inversion can be expressed as a minimization problem.[17] Given the vector of experimental observations, $\mathbf{y}^{\mathrm{obs}}$, and the vector of model predictions, $\mathbf{y}^{\mathrm{calc}}(\mathbf{k})$, (i.e., depending explicitly on the vector of unknown parameters, $\mathbf{k}$, and implicitly on the known parameters, θ) we define a cost function $J(\mathbf{k})$,

$$J(\mathbf{k}) \equiv \sum_{a}^{A}\sum_{b}^{B} \begin{cases} 0 & |y_{ab}^{\mathrm{obs}} - y_{ab}^{\mathrm{calc}}| \le \epsilon_{ab} \\ \left(\dfrac{y_{ab}^{\mathrm{obs}} - y_{ab}^{\mathrm{calc}}(\mathbf{k})}{y_{ab}^{\mathrm{obs}}}\right)^2 & |y_{ab}^{\mathrm{obs}} - y_{ab}^{\mathrm{calc}}| > \epsilon_{ab} \end{cases} \quad (1)$$

where ϵ_{ab} is the experimental error in the measurement of y_{ab}^{obs}. Here, the indices $a = 1, 2, ..., A$ and $b = 1, 2, ..., B$ refer, respectively, to the discrete data sample times and the observed species.

Because we desire to find the distribution of parameter vectors, $\mathbf{k}$, consistent with the data, we must perform a global minimization of $J(\mathbf{k})$ on the domain of $\mathbf{k}$. Although techniques such as gradient descent can very efficiently locate local minima, only a thorough sampling of the function over the entire domain ensures that we find the distribution of minima consistent with the data and its errors. If the calculation of $J(\mathbf{k})$ is expensive, then the cost function evaluation will limit the optimization methods that can be employed, often preventing the use of global techniques.

Furthermore, convergence to a local minimum, which is often used as an a posteriori verification that a minimization algorithm was successful, is not necessarily informative. Because each measurement, y_{ab}^{obs}, is accurate only within some tolerance, ϵ_{ab}, there could be a large set of solutions, $\mathbf{k}^{\mathrm{opt}}$, that satisfy the condition

$$|y_{ab}^{\mathrm{obs}} - y_{ab}^{\mathrm{calc}}(\mathbf{k}^{\mathrm{opt}})| \le \epsilon_{ab} \quad (2)$$

Each of these solutions, $\mathbf{k}^{\mathrm{opt}}$, is a local minimum of the cost function, $J(\mathbf{k})$, such that $J(\mathbf{k}^{\mathrm{opt}}) = 0$.

To evaluate the cost function, $J(\mathbf{k})$, for a trial set of parameters, $\mathbf{k}$, a means for calculating values of the observed concentrations, $\mathbf{y}^{\mathrm{calc}}$, must be available. In the present study, the chemical system is taken as spatially homogeneous, such that the concentrations of the species are described by a set of temporal differential equations of the form

$$\frac{\mathrm{d}\mathbf{x}}{\mathrm{d}t} = h(\mathbf{x},\mathbf{k};\theta) \quad (3)$$

where $\mathbf{x}$ is the vector of concentrations of all species, $x_1, x_2, ..., x_S$. We will assume that the vector of known parameters, θ, includes the initial concentrations of the reactants, the temperature (taken as constant), and all known rate constants. Because the known parameters, θ, are included implicitly in the model, the vector $\mathbf{x}$ is dependent only on the unknown rate constants, $\mathbf{k}$, and time,

$$\mathbf{x} = \mathbf{x}(\mathbf{k},t) \quad (4)$$

The coupled eqs 3 were integrated using the LSODE integrator, which is based on the algorithm due to Gear.[18,19] Let $X_1, X_2, ..., X_B$ be the B observable species whose concentrations were measured at times $t_1, t_2, ..., t_A$. The model generates the vector $\mathbf{y}^{\mathrm{calc}}$ with components

$$y_{ab}^{\mathrm{calc}}(\mathbf{k}) = x_b(\mathbf{k},t_a) \quad (5)$$

for $a = 1,2, ..., A$ and $b = 1, 2, ..., B$. The value of $J(\mathbf{k})$ in eq 1 can be evaluated for any set of trial parameters $\mathbf{k}$ in the specified parameter space. However, direct evaluation of $J(\mathbf{k})$ involves numerical integration of the kinetic equations for the system, which can be computationally expensive.

Reduction of the cost of inversion can be accomplished through the creation of a map function. Let $f_{ab}(\mathbf{k})$ be a suitable map function for $y_{ab}^{\mathrm{calc}}(\mathbf{k})$ that meets the requirements (a), (b), and (c) listed in section I. Then,

$$y_{ab}^{\mathrm{calc}}(\mathbf{k}) \approx f_{ab}(\mathbf{k}) \quad (6)$$

for replacement in eq 1. Once such a map function is generated, minimization of eq 1 can be performed on the map function rather than on the calculated function. To ensure that the map function inversion yields accurate results, we require that the error of the map function approximation be negligible compared to the experimental measurement errors, ϵ_{ab}. If this criterion is met, then the optimal parameters obtained from the inversion of the map function will be an accurate approximation to the results that would have been obtained by an inversion of the parent model. However, the efficiency of the inversion process will be greatly improved because each expensive model evaluation is replaced with a map evaluation. To ensure accuracy in the inversion, a final round of optimization may be performed using $y_{ab}^{\mathrm{calc}}(\mathbf{k})$ starting with the distribution of optimal parameters found with the map.

To meet criterion (b) for a feasible map function, the overhead required to generate the map must be considered. Determining the value of $f_{ab}(\mathbf{k})$ for an arbitrary $\mathbf{k}$ in the domain $\mathscr{K}$ is an N-dimensional interpolation problem, for which many algorithms are known.[20] In low dimensions, interpolation is extremely fast and by increasing the sampling, s, the interpolation can be made arbitrarily accurate. Unfortunately, the number of sample points needed to generate a look-up table to perform N-dimensional interpolation grows as s^N, where s is the number of points sampled per dimension. Thus, the overhead of map generation and the cost of map evaluation by this direct approach quickly become excessive.

An accurate, efficient map that does not require excessive sampling can be obtained through the use of the HDMR algorithm. Given an N-dimensional model function $y^{\mathrm{calc}}(\mathbf{k})$ (where the a and b indices are suppressed for notational convenience) defined on a hypercubic domain $\mathscr{K}$,

$$\mathscr{K} \equiv \{\mathbf{k} | k_1^{\min} \le k_1 \le k_1^{\max}, k_2^{\min} \le k_2 \le k_2^{\max}, ..., k_N^{\min} \le k_N \le k_N^{\max}\} \quad (7)$$

we can rewrite $y^{\mathrm{calc}}(\mathbf{k})$ in the following form[10,21]

$$y^{\mathrm{calc}}(\mathbf{k}) \equiv [f_0 + \sum_{i}^{N} f_i(k_i) + \sum_{i<j} f_{ij}(k_i,k_j)] + ... + f_{1,2,...,N}(k_1,k_2,...,k_N) \quad (8)$$

where f_0 is a constant, the term $f_i(k_i)$ describes the dependence of the output on the independent action of k_i, the term $f_{ij}(k_i,k_j)$ describes the dependence of the output on the nonseparable,

cooperative action of k_i and k_j, and higher order terms describe the dependence of the output on the cooperative action of three or more variables. This form is exact because the last term $f_{1,2...,N}(k_1,k_2,...,k_N)$ can capture any residual cooperative action involving all the variables.

The central assumption of HDMR is that higher order cooperation is insignificant in well-defined physical systems and eq 8 may be truncated to low order without sacrificing accuracy or nonlinearity. An Lth-order HDMR is obtained by truncating all terms describing correlation of more than L variables. For instance, a second-order HDMR expansion, $f(\mathbf{k})$, would have included only the bracketed terms in eq 8,

$$f(\mathbf{k}) = f_0 + \sum_{i}^{N} f_i(k_i) + \sum_{i<j} f_{ij}(k_i,k_j) \tag{9}$$

It has been found that for many physical systems a second-order HDMR approximation is sufficiently accurate over the domains of interest.[10,15,16]

The HDMR expansion functions can be obtained in several ways.[22] We have chosen to evaluate the HDMR functions with respect to a nominal point, $\bar{\mathbf{k}}$, known as the "cut-center". The terms in the expansion are defined as follows,

$$f_0 \equiv y^{\text{calc}}(\bar{k}_1,\cdots,\bar{k}_N) \tag{10}$$

$$f_i(k_i) \equiv y^{\text{calc}}(\bar{k}_1,\cdots,k_i,\cdots,\bar{k}_N) - f_0 \tag{11}$$

$$f_{ij}(k_i,k_j) \equiv y^{\text{calc}}(\bar{k}_1,\cdots k_i,\cdots,k_j\cdots,\bar{k}_N) - f_i(k_i) - f_j(k_j) \tag{12}$$

where $\cdots$ denotes all arguments set to their cut-center values. The terms in an HDMR expansion can be viewed as low-dimensional cuts of the function domain $\mathcal{K}$ through the cut-center point. The constant f_0 is defined to be the value of the function y^{calc} at the cut-center. The first-order functions f_i are evaluated by sampling the function y^{calc} along the k_i axis through the cut-center and then subtracting off the contribution of f_0. The second-order functions f_{ij} are evaluated by sampling the function y^{calc} in the k_i,k_j-plane through the cut-center and subtracting off zeroth-order and first-order contributions. It is also possible to define HDMR expansions at multiple cut-centers within the domain $\mathcal{K}$. By creating several local maps rather than a single global map, we can sometimes increase the overall model approximation accuracy and efficiency.[23]

Two important issues of a general nature must be addressed during the HDMR generation stage of the algorithm. First, the order of the HDMR map needed to achieve sufficient accuracy must be determined. In general, an Lth-order HDMR requires $O(s^L N^L)$ function evaluations. The HDMR representation effectively reduces the original problem of interpolating in N dimensions down to performing interpolation over a set of L-dimensional subspaces with $L \ll N$. Thus, the sampling cost has been reduced from exponential to polynomial scaling. Increasing the order of the HDMR expansion improves map accuracy at the cost of a decrease in computational efficiency. In the present studies, sufficient accuracy was found for second-order maps. As a second issue, the domain, $\mathcal{K}$, of the HDMR map must be specified. A large domain is desirable to capture as much of the parameter space as possible. Unfortunately, increasing the size of the domain often reduces map accuracy. Ideally, the HDMR map is large enough to include all of the parameter space of interest, while still being accurate enough to perform a valid inversion.

Issues of HDMR order and domain size are problem dependent due to the possibly different behavior of each kinetic system. Before or during the inversion, the accuracy of the HDMR maps should be tested as an intrinsic part of the overall inversion algorithm. In this work, we have tested the error of each HDMR map through random sampling on the parameter domain, $\mathcal{K}$, to ensure that the map error is negligible compared to the uncertainties in the experimental data subject to inversion. The details of this process will be described in section III.

Because a global inversion of the parameter space is needed to identify multiple minima, we chose to use the steady-state genetic algorithm described by Goldberg to perform the map inversion.[9,24] Global sampling is made feasible by the efficiency of the map functions. The end result of a successful genetic algorithm inversion is not a single solution but a family of multiple solutions all of which satisfy eq 2, thereby providing a distribution of model parameters consistent with the laboratory data.

Section III provides three illustrations of the HDMR map inversion process. The first test case had linear, first-order reaction kinetics. This system was used to explore the dependence of map accuracy on domain size and other map parameters. The second system, the reaction of H_2 with Br_2, probed the quality of the inverted rate constants with respect to the completeness of the input data and experimental error. Finally, results obtained from the inversion of data from the reaction of formaldehyde with OH were compared with earlier results.[2]

III. Illustrations

The methodology presented in section II can be applied to any kinetic inversion problem, but the efficiency of the inversion depends on the accuracy of the maps. A series of quasi-local maps can be very effective in overcoming the error in any particular map,[23] but here we focus on utilizing a single global map. It is therefore necessary to know how map accuracy is related to the order of the HDMR approximation and the domain size. To this end, the map inversion algorithm described in section II was applied to three different kinetic systems.

A. Linear Kinetic System. The first test of the algorithm was performed on a system of linear kinetic equations. Linear kinetic processes occur in many real systems, including hydrocarbon cracking.[25] The word "linear" refers only to the chemical kinetics, and not to the map functions $f_{ab}(\mathbf{k})$, which can be highly nonlinear. The linear kinetic equations are prescribed by the mechanism[26]

$$\begin{array}{llll} X_1 \rightleftharpoons X_2 & & & \\ X_1 \rightleftharpoons X_3 & X_2 \rightleftharpoons X_3 & & \\ \vdots & \vdots & \ddots & \\ X_1 \rightleftharpoons X_S & X_2 \rightleftharpoons X_S & \cdots & X_{S-1} \rightleftharpoons X_S \end{array} \tag{13}$$

This mechanism produces a system of equations,

$$\frac{d\mathbf{x}}{dt} = \mathbf{M}\mathbf{x} \tag{14}$$

where the elements of the $\mathbf{M}$ matrix are

$$m_{ij} = \begin{cases} k'_{j,i}, & i \neq j \\ -\sum_{l,l\neq i} k'_{i,l}, & i = j \end{cases} \tag{15}$$

TABLE 1: Confidence Intervals for the Distribution of the Extracted Parameters from the Linear Kinetic Inversion

	k'_1	k'_2	k'_3	k'_4	k'_5	k'_6
target values (sec^{-1})	0.80	0.31	0.57	0.19	0.22	0.24
68% confidence	[0.76, 0.83]	[0.27, 0.32]	[0.50, 0.64]	[0.08, 0.26]	[0.34, 0.74]	[0.14, 0.32]
90% confidence	[0.74, 0.85]	[0.26, 0.34]	[0.46, 0.66]	[0.07, 0.28]	[0.19, 0.82]	[0.09, 0.33]

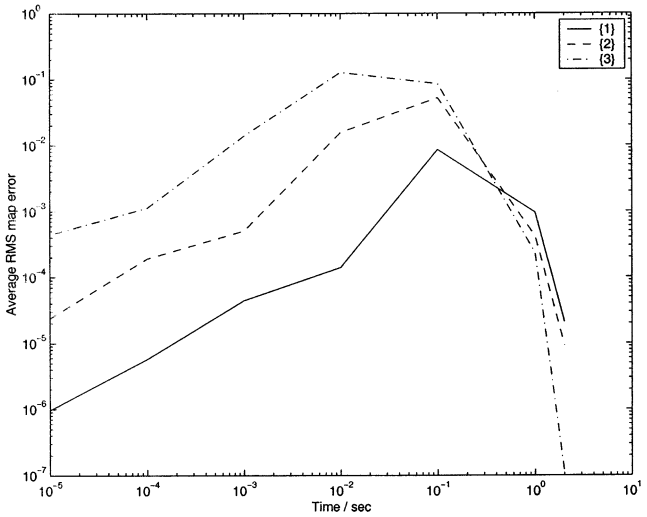

Figure 1. Map error versus time for the linear kinetic system. The accuracy of the HDMR map was dependent on both the sample time and the size of the domain $\mathcal{K} = \{i\}$ over which the map was created.

and where the rate constant k'_{ij} corresponds to the reaction, $X_i \rightarrow X_j$. Equation 14 has the solution,

$$\mathbf{x}(t) = e^{\mathbf{M}t}\mathbf{x}(0) \tag{16}$$

We note that the rate constants k'_{ij} and k'_{ji} corresponding to the forward and reverse reactions, $X_i \rightarrow X_j$ and $X_j \rightarrow X_i$, are related by detailed balance,

$$k'_{i,j}e^{(G_j^f - G_i^f)/2RT} = k'_{j,i}e^{(G_i^f - G_i^f)/2RT} \tag{17}$$

where T is the temperature, R is the ideal gas constant, and G_i^f and G_j^f are the free energies of species X_i and X_j, respectively. The temperature, T, the initial concentrations, $x_1(0)$, $x_2(0)$, ..., $x_S(0)$, and the free energies, G_1^f, G_2^f, ..., G_S^f, were treated as the known parameters, θ. Rather than perform a constrained optimization with eq 17 on the original rate constants, the $S \times S$ diagonal transformation matrix $\mathbf{T}$ is introduced such that

$$t_{ii} = e^{-G_i^f/2RT} \tag{18}$$

From eq 17,

$$\mathbf{M} = \mathbf{T}^{-1}\mathbf{P}\mathbf{T} \tag{19}$$

where $\mathbf{P}$ is a symmetric matrix. So eq 16 can be rewritten as

$$\mathbf{x}(t) = \mathbf{T}^{-1}e^{\mathbf{P}t}\mathbf{T}\mathbf{x}(0) \tag{20}$$

The $N = S(S-1)/2$ upper-triangular elements of $\mathbf{P}$ are the new, unconstrained parameters sought after by inversion. Because rate constants can vary over many orders of magnitude, the HDMR variables were scaled logarithmically with respect to the rate constants. Thus, the unknown model parameters, k_1, k_2, ..., k_N, used for HDMR map construction were the logarithms of the N off-diagonal elements of $\mathbf{P}$: $k_1 = \log_{10}(p_{12})$, $k_2 = \log_{10}(p_{13})$, ..., $k_N = \log_{10}(p_{(S-1)S})$. Finally, combining eqs 5 and 20, we obtain

TABLE 2: Root Mean Squared Relative Error for the Set of Maps Describing Each System Calculated Using Eq 22 by a Random Sample of $R = 1000$ Test Points[a]

	first-order maps	second-order maps
linear, $S = 4$, {1}	0.05	0.009
HBr, data set I {0.5}	0.03	0.004
HBr, data set II {0.5}	0.04	0.003
HBr, data set III {0.5}	0.07	0.009
formaldehyde, partial {2}	0.12	0.01
formaldehyde, full	0.29	0.03

[a] $\mathcal{K} = \{i\}$ is the logarithmic domain size along each axis K_i.

$$y_{ab}^{calc}(\mathbf{k}) = \sum_j (e^{(\mathbf{T}^{-1}\mathbf{P}(\mathbf{k})\mathbf{T})t_a})_{bj}x_j(0) \tag{21}$$

The linear system studied involved $S = 4$ species with $N = 6$ parameters, $\mathbf{k}'$, given in Table 1, with the tilde label denoting the true (target) value of the constants. The experimental data to be inverted was simulated using the kinetics model from eq 21 with arbitrary initial conditions away from equilibrium. The simulated experimental data vector $\mathbf{y}^{obs}$ consisted of the concentrations of all four species ($B = 4$) sampled at $A = 20$ intervals over the range $t = 0$ s to $t = 0.2$ s.

The map accuracy was determined with respect to the parameter domain size and the time of reaction. The domain, $\mathcal{K}$, of the parameters, $\mathbf{k}$, in eq 7 is related logarithmically to the elements of the matrix $\mathbf{P}$. Hence, a uniform domain of size $\mathcal{K} = \{2\}$ spans 2 orders of magnitude with respect to the off-diagonal elements of $\mathbf{P}$. The accuracy of a set of HDMR maps, $f_{ab}(\mathbf{k})$ for all a and b, was characterized by its root-mean-squared relative error. R random points, $\mathbf{k}_1$, $\mathbf{k}_2$, ..., $\mathbf{k}_R$, were sampled from the domain $\mathcal{K}$. For each point $\mathbf{k}_r$, the value of y_{ab}^{calc} was generated using eq 21 and the average RMS relative error per sample point E_{RMS}^{av} of the maps was given by

$$E_{RMS}^{av.} = \sqrt{\frac{1}{ABR}\sum_a^A\sum_b^B\sum_r^R\left(\frac{y_{ab}^{calc}(\mathbf{k}_r) - f_{ab}(\mathbf{k}_r)}{y_{ab}^{calc}(\mathbf{k}_r)}\right)^2} \tag{22}$$

Table 2 gives E_{RMS}^{av} for the sets of maps used in each of the systems studied, including those used in the present case with domain $\mathcal{K} = \{1\}$. In all cases, the second-order maps were of excellent accuracy over a significant dynamic range of the parameter spaces.

Using the cut-HDMR algorithm described in section II, second-order HDMR maps were generated for the concentrations of all four species X_1, X_2, X_3, and X_4 at a series of sample times.

It was found that map accuracy decreased as the size of the parameter domain increased. Furthermore, the map accuracy exhibited a dependence on the time of observation. Figure 1 shows the dependence of map accuracy on domain size and time of observation. Near $t = 0$ and $t \rightarrow \infty$, the maps were naturally accurate for simple physical reasons. Near $t = 0$, the concentrations of all species were close to their initial concen-

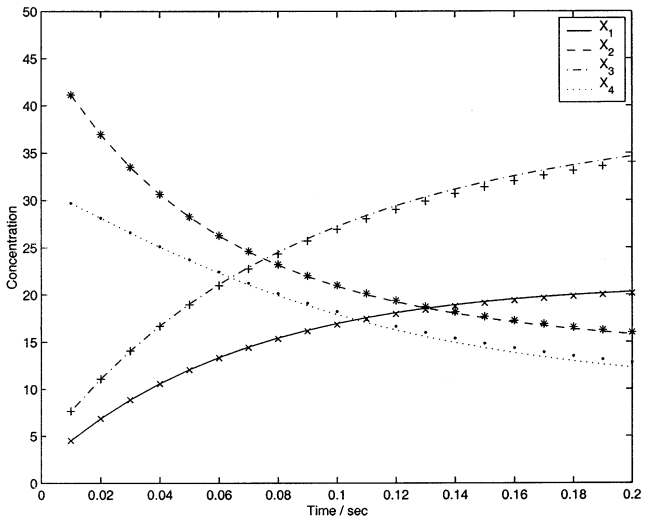

Figure 2. Illustration of species concentrations versus time for the linear kinetic system calculated from the original kinetic model (lines) and from the HDMR maps (points).

trations, which are specified by the f_0 term in eq 9, whereas for $t \rightarrow \infty$ the system approaches its equilibrium concentrations, which are independent of the rate constants.

The inversion was performed on a domain $\mathscr{K} = \{1\}$ with second-order maps that produced an RMS error of <1% for each sample time. A total of 80 HDMR maps of second-order were generated by describing the concentrations of the $B = 4$ species sampled at $A = 20$ intervals over the range $t = 0$ s to $t = 0.2$ s. Figure 2 compares the results of model evaluation to map evaluation for the concentrations arising from a randomly selected set of parameters on the domain.

The map-facilitated inversion was performed with a steady-state genetic algorithm using 100 noninteracting populations each containing 100 individuals. This large-scale search was performed to ensure a reliable identification of the full family of rate constants consistent with the data. The genetic algorithm was run for 100 generations and involving a total of 4.4×10^6 map evaluations. Each population converged to a distinct solution for $\mathbf{k}$, which minimized the value of the cost function $J(\mathbf{k})$ in eq 1. The present simulations took the data as ideal with no measurement error (i.e., $\epsilon_{ab} = 0$), but a finite amount of data will generally still produce a distribution of consistent model parameters. The genetic algorithm found the set of solutions that minimized the average RMS error between the experimental data and the map prediction. The solutions identified had J values ranging from 2.4×10^{-5} to 3.4×10^{-3}, corresponding to average RMS errors of 5.5×10^{-5} and 6.5×10^{-3}, respectively. Figure 3 shows the distribution for three of the parameters: k_1, k_2, and k_5.

A statistical measure such as sample variance could be used to characterize these distributions, but this measure is misleading due to the nonlinearity of the inverse problem, which generally produces a nonnormal distribution (cf., the distribution for k_5 in Figure 3). Instead, these distributions were characterized using confidence intervals.[14,23] Table 1 shows the confidence intervals for the inverted parameters. Although the extracted parameters are clustered around the target values, $\tilde{\mathbf{k}}$, which were used to generate the data, there are a wide range of values consistent with the experimental data. The determination of such true parameter distributions should be the goal in any reliable inversion, and this information will generally only be available through the use of maps permitting large numbers (more than 10^6 in the present case) of system evaluations.

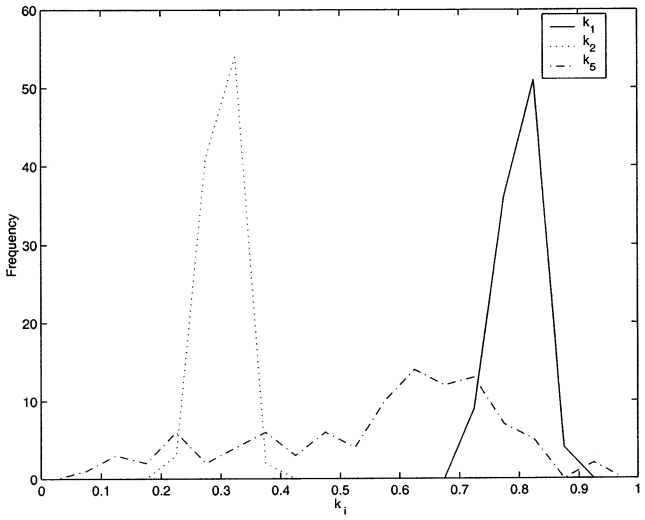

Figure 3. Histogram of the distribution of the extracted parameters k_1, k_2, and k_5 for the linear kinetic system. From Table 1 the target values for these parameters are respectively 0.80, 0.31, and 0.57. The distribution is tightly clustered around the target values for k_1 and k_2. On the other hand, k_5 was poorly defined by the experimental data. See Table 1 for the target values.

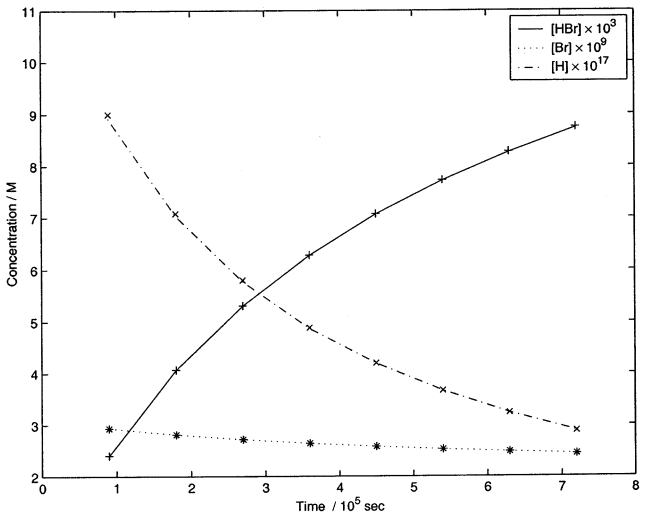

Figure 4. Species concentrations versus time for the HBr kinetic system calculated from the original kinetic model (lines) and from the HDMR maps (points).

B. H_2 + Br_2 Reaction. The second kinetic system that we investigated was the oxidation of H_2 by Br_2 to form HBr. This reaction has been studied for a long time,[27] and we adopted the following mechanism,[28]

$$\begin{aligned}
\mathrm{Br_2} &\rightarrow \mathrm{Br^\bullet + Br^\bullet} & k_1' &= 1.58 \times 10^{-6}\ \mathrm{s^{-1}} \\
\mathrm{Br^\bullet + Br^\bullet} &\rightarrow \mathrm{Br_2} & k_2' &= 1.34 \times 10^{9}\ \mathrm{L\ mol^{-1}\ s^{-1}} \\
\mathrm{Br^\bullet + H_2} &\rightarrow \mathrm{HBr + H^\bullet} & k_3' &= 7.08 \times 10^{2}\ \mathrm{L\ mol^{-1}\ s^{-1}} \\
\mathrm{HBr + H^\bullet} &\rightarrow \mathrm{Br^\bullet + H_2} & k_4' &= 7.08 \times 10^{9}\ \mathrm{L\ mol^{-1}\ s^{-1}} \\
\mathrm{Br^\bullet + HBr} &\rightarrow \mathrm{Br_2 + H^\bullet} & k_5' &= 2.51 \times 10^{10}\ \mathrm{L\ mol^{-1}\ s^{-1}} \\
\mathrm{Br_2 + H^\bullet} &\rightarrow \mathrm{Br^\bullet + HBr} & k_6' &= 2.09 \times 10^{-8}\ \mathrm{L\ mol^{-1}\ s^{-1}}
\end{aligned} \tag{23}$$

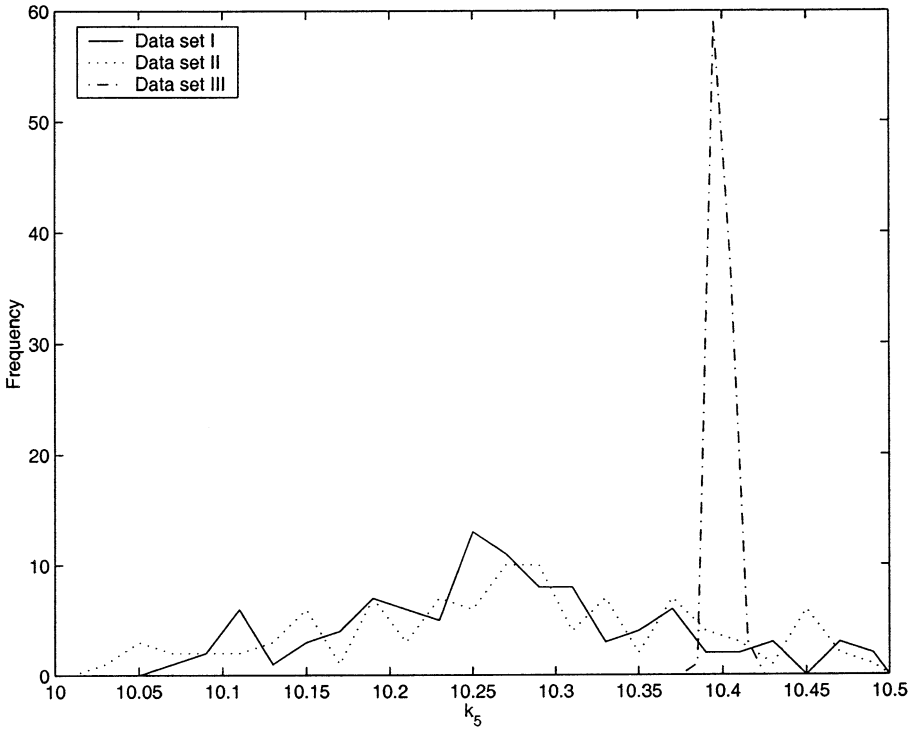

Figure 5. Distribution of extracted values for k_5 in the HBr system using the three different sets of simulated, error-free data. The true value of the parameter is $k_5 = 10.40$.

The experimental data were simulated by specifying the initial concentrations and temperature from the original work by Bodenstein and Lind.[27] The target values for the unknown rate constants, $\mathbf{k}'$, were the literature values listed in eq 23.[28−30] Because the values of the rate constants differed by many orders of magnitude, the HDMR variables, $\mathbf{k}$, were again scaled logarithmically with respect to the rate constants, $\mathbf{k}'$.

The simulated data, $\mathbf{y}^{obs}$, were generated by numerically integrating the differential equations associated with the mechanism in eq 23 using LSODE.[18] Eight samples were taken between $t = 0$ s and $t = 7.2 \times 10^5$ s, and the data were divided into categories I, II, and III. Data set I contained only the concentration of HBr at each measurement, data set II included HBr and Br$^\bullet$, and data set III included the concentrations of HBr, Br$^\bullet$, and H$^\bullet$. Thus, the three simulated experiments contained 8, 16, and 24 data points, respectively, permitting an analysis of the influence of the nature of the experimental data on rate constant inversion. The influence of experimental error, ϵ_{ab} in eq 1, on the distribution of the inverted rate constants was also investigated.

An analysis of map accuracy versus domain size was performed with maps constructed for the concentrations of HBr, Br$^\bullet$, and H$^\bullet$ at the eight sample times. It was found that for a domain of size $\mathscr{K} = \{0.5\}$, second-order maps could model the data from data sets I, II, and III with an average RMS error of 0.35%, 0.29%, and 0.91%, respectively (see Table 2). Thus, the maps provided an excellent approximation of the full kinetic model within the specified parameter domain. Figure 4 compares the results of model versus map evaluation for concentrations using a randomly selected set of parameters on the domain.

Separate inversions of the data simulated in data sets I, II, and III were performed using the same methodology applied in section IIIA. Initially, all experimental measurements were assumed to be exact ($\epsilon_{ab} = 0$) and a set of 100 best-fit solutions to the experimental data were generated for each data set. All of the best solutions identified by the genetic algorithm produced concentrations that agreed with the data points within an average RMS error of <1%.

The effect of the extra data points present in cases II and III was significant. Figure 5 shows the distribution of values for k_5 obtained from the three inversions. k_5 was not well-defined by data sets I and II but was accurately identified by III. Clearly, the value of k_5 is sensitive to H$^\bullet$, which was observed in data set III. Similar dependencies were found between k_4 and H$^\bullet$ and k_3 and Br$^\bullet$.

The inclusion of experimental error in the inversion process naturally will affect the distributions of inverted parameter values. The average RMS relative error of the best solutions in the $\epsilon_{ab} = 0$ inversion arising from the finite amount of data ranged from 0.092% to 0.76%. Simulated experimental error was then introduced through ϵ_{ba} and the inversions were rerun. When the experimental error was set to 2% or more, then all of the genetic algorithm populations converged to a solution for which $J(\mathbf{k}) = 0$ (i.e., the experimental data were fit within the specified tolerance at every data point). Figure 6 shows the distributions of values for k_5 obtained from data set III with $\epsilon_{ab} = 0\%$, 2%, and 5% for each data point. In general, greater error in the experimental data produced a broader distribution of values of the parameters. Similar distribution broadening was observed for all three sets of experimental data and for all six rate constants.

C. Oxidation of Formaldehyde. The HDMR map inversion algorithm was tested on the oxidation of formaldehyde by OH, because an extensive inversion of this system was performed using a linear sensitivity analysis method.[2] The formaldehyde system is described by a set of 17 reactions involving 15

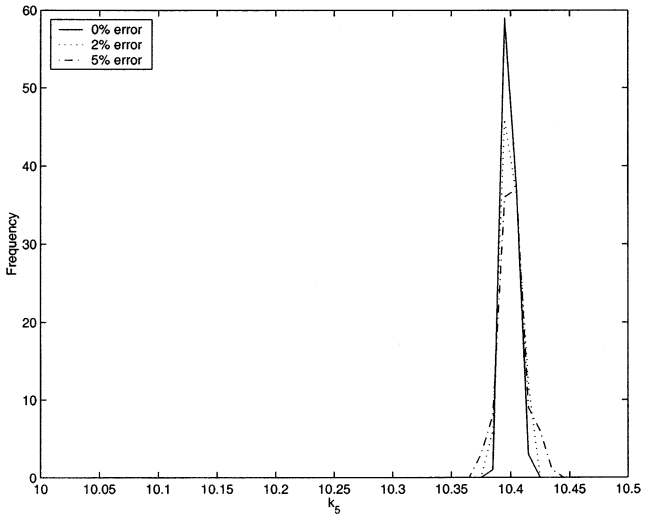

Figure 6. Distribution of extracted values for k_5 in the HBr system using simulated data set III with errors of 0%, 2%, and 5%.

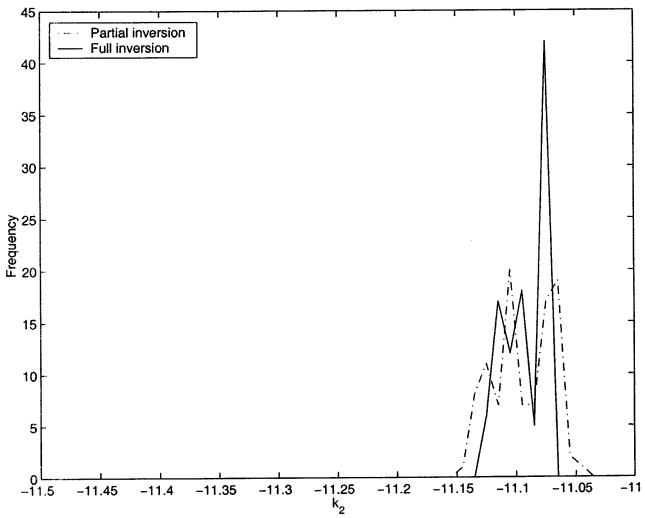

Figure 7. Distribution of the extracted values for k_2 in the formaldehyde system using a full and partial inversion technique.

chemical species,[2]

$$\mathrm{H + NO_2 \rightarrow OH + NO} \quad 1.28 \times 10^{-10}\ \mathrm{cm^3 molecule^{-1} s^{-1}}$$

$$\mathrm{OH + H_2CO \rightarrow H_2O + HCO} \quad k_2'$$

$$\mathrm{HCO + NO_2 \rightarrow H + CO_2 + NO} \quad 4.00 \times 10^{-11}\ \mathrm{cm^3\ molecule^{-1}\ s^{-1}}$$

$$\mathrm{HCO + O_2 \rightarrow HO_2 + CO} \quad 5.50 \times 10^{-12}\ \mathrm{cm^3\ molecule^{-1}\ s^{-1}}$$

$$\mathrm{HO_2 + NO \rightarrow OH + NO_2} \quad 8.30 \times 10^{-12}\ \mathrm{cm^3\ molecule^{-1}\ s^{-1}}$$

$$\mathrm{H + O_2(+M) \rightarrow HO_2(+M)} \quad 5.44 \times 10^{-15}\ \mathrm{cm^3\ molecule^{-1}\ s^{-1}}$$

$$\mathrm{H + H_2CO \rightarrow H_2 + HCO} \quad 6.69 \times 10^{-14}\ \mathrm{cm^3\ molecule^{-1}\ s^{-1}}$$

$$\mathrm{OH + HCO \rightarrow H_2O + CO} \quad 5.00 \times 10^{-11}\ \mathrm{cm^3\ molecule^{-1}\ s^{-1}}$$

$$\mathrm{H + HCO \rightarrow H_2 + CO} \quad 5.00 \times 10^{-11}\ \mathrm{cm^3\ molecule^{-1}\ s^{-1}}$$

$$\mathrm{H \rightarrow destruction} \quad 10\ \mathrm{s^{-1}}$$

$$\mathrm{OH \rightarrow destruction} \quad 5\ \mathrm{s^{-1}}$$

$$\mathrm{HCO \rightarrow destruction} \quad 10\ \mathrm{s^{-1}}$$

$$\mathrm{HO_2 \rightarrow destruction} \quad 10\ \mathrm{s^{-1}}$$

$$\mathrm{OH + OH \rightarrow H_2O + O} \quad 1.99 \times 10^{-12}\ \mathrm{cm^3\ molecule^{-1}\ s^{-1}}$$

$$\mathrm{OH + HO_2 \rightarrow H_2O + O_2} \quad 6.40 \times 10^{-11}\ \mathrm{cm^3\ molecule^{-1}\ s^{-1}}$$

$$\mathrm{H + HO_2 \rightarrow OH + OH} \quad 7.00 \times 10^{-11}\ \mathrm{cm^3\ molecule^{-1}\ s^{-1}}$$

$$\mathrm{OH + H_2CO \rightarrow HCOOH + H} \quad k_{17}' \qquad (24)$$

The methodology employed earlier[2] extracted only k_2' and k_{17}' with the other 15 rate constants treated as known and assigned literature values. Because these latter 15 rate constants were specified only within some confidence interval, their uncertainty contributed to the uncertainty of the extracted values of k_2' and k_{17}'. In the previous paper, the uncertainty analysis was carried out using a linear sensitivity analysis. In the present work, two HDMR-facilitated inversions were carried out with different assumptions and conditions.

The first HDMR map inversion was designed to follow the earlier procedure[2] as closely as possibie. The experimental data for inversion were generated by numerical integration of the model equations using the best-fit values for $\mathbf{k}'$ reported previously:[2] $k_2' = 7.75 \times 10^{-12}$ cm^3 molecule^{-1} s^{-1} and $k_{17}' = 2.00 \times 10^{-13}$ cm^3 molecule^{-1} s^{-1}. These simulated data are very close to the actual laboratory data for the system,[2] and they therefore provide a realistic test of the HDMR algorithm. The data consisted of the OH radical concentration at 10 sample times for 11 runs under different reaction conditions. The reaction conditions used for each run are the same as those in Table 2 of the article by Yetter et al.[2] In addition, the reported 5% experimental error in the measurement of OH was used as the error tolerance, ϵ_{ab}, for the HDMR-based inversion. The HDMR variables were scaled logarithmically with respect to the model rate constants.

The first inversion treated rate constants k_1', k_2', k_4',..., k_{16}' as known parameters that were set to their literature values. A set of second-order HDMR maps using only k_2 and k_{17} as variables with a domain size of $\mathscr{K} = \{2\}$ was generated for each OH concentration, y_{ab}^{calc}. In this case, the index b refers to the 11 runs under different reaction conditions. A modification was made in the inversion procedure to take into account the uncertainty inherent in the values of the known rate constants.

Because the values of the parameters, θ, were not known exactly, the errors associated with the values of θ affected the values obtained for k_2' and k_{17}'. Instead of approximating the propagation of errors using linear sensitivity analysis, we used the efficiency of the HDMR maps to perform a Monte Carlo analysis of the error propagation, as suggested by Alper et al.[14] A set of values for the known rate constants, θ, was selected from a uniform distribution over their reported confidence intervals.[2] Then second-order HDMR maps were generated using k_2 and k_{17} as the HDMR variables. Finally, these maps were inverted using the genetic algorithm to find a single, best solution. By repeating this process 100 times, a distribution of best solutions was generated for k_2 and k_{17}. These distributions reflected both the effects of the 5% error in the experimental measurements, $\mathbf{y}^{\mathrm{obs}}$, and the effects of error in the selected values of the known parameters, θ, on k_2 and k_{17}.

Figures 7 and 8 show the distributions of k_2 and k_{17} generated by this partial inversion. The average values obtained for k_2' and k_{17}' were 8.0×10^{-12} and 2.0×10^{-13}, compared to 7.8×10^{-12} and 2.0×10^{-3} reported by Yetter et al.[2] The confidence

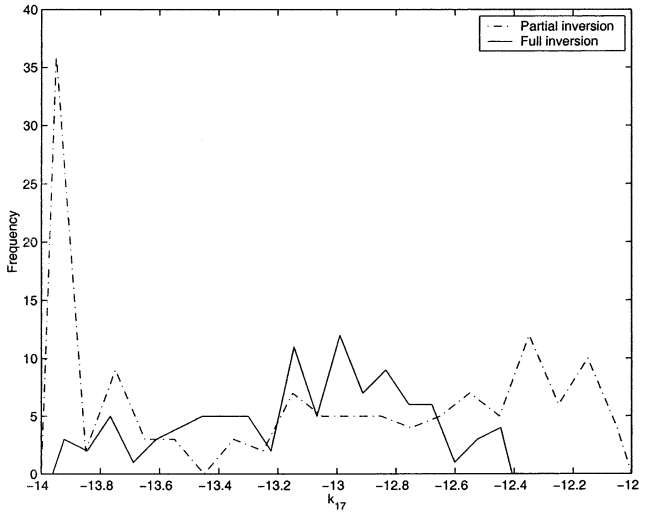

Figure 8. Distribution of extracted values for k_{17} in the formaldehyde system using a full and partial inversion technique.

intervals obtained by the partial inversion and those reported by Yetter et al. were also similar. In both studies, k_2' was found to be well-defined and k_{17}' was found to be poorly defined by the experimental data. However, it should be noted that only 10 out of the 100 solutions generated by the partial inversion had J values of 0. The J values associated with the other 90 solutions generated ranged from 1.1×10^{-2} to 1.7, corresponding to average RMS relative errors of 1.0×10^{-2} and 1.3×10^{-1}, respectively.

Because the nominal values of the known rate constants were selected from a uniform distribution over their confidence intervals before each inversion, they often differed substantially from their true values, i.e., the values that had been used to generate the simulated experimental data. In the limit of an arbitrarily large number of inversions, the correct values of these parameters could be determined. However, in this limit the "known" parameters should be treated as variables subject to inversion over the domain of their confidence intervals by performing a full inversion rather than a partial inversion. The HDMR mapping technique provides an efficient means to perform a full inversion over all rate constants.

In the full inversion, the variables k_1, k_3, k_4, ..., k_{16} were inverted over the domain of their reported uncertainties. A larger domain could have been searched, but it was assumed that the uncertainty ranges reported in the literature were accurate, i.e., the real values of k_1, k_3, k_4, ..., k_{16} fell within the literature uncertainties. On the other hand, the two variables k_2 and k_{17} were inverted over a domain of 2 orders of magnitude to ensure as general an inversion as possible.

Table 2 shows the accuracy of the maps obtained for the full and partial inversions. Figures 7 and 8 compare the distributions obtained for k_2 and k_{17} by the full inversion to the distributions obtained by the partial inversion. Unlike the solutions generated by the partial inversion, of which only 10 modeled the experimental data within the specified tolerances, all 100 of the solutions generated by the full inversion modeled the data perfectly ($J = 0$) within the stated data error limits. This result implies that the information provided by $\mathbf{y}^{obs}$ specified k_1, k_3, k_4, ..., k_{16} to greater accuracy than their literature uncertainties! This behavior points out that caution is called for in considering the standard procedure of fixing a subset of the rate constants at prior determined nominal values while aiming to extract a small set of the remainder. Although this procedure seems logical, it can introduce hidden inconsistencies that show up as possible false error in the extracted rate constants. The ability to employ high-speed, accurate maps relieves this problem to allow for an efficient, full and consistent inversion with each of the extracted parameters left as free to set its true distribution consistent with the data.

TABLE 3: Efficiency of Model Evaluation vs Map Evaluation[a]

	model evaluation	HDMR evaluation
linear	3.2×10^{-3}	9.7×10^{-2}
HBr, data set I	1.1×10^{-2}	3.5×10^{-2}
HBr, data set II	1.2×10^{-2}	4.0×10^{-2}
HBr, data set III	1.1×10^{-2}	4.7×10^{-2}
formaldehyde, partial	2.5×10^{-1}	6.8×10^{-3}
formaldehyde, full	2.5×10^{-1}	8.4×10^{-2}

[a] Values given in seconds/evaluation.

Although the three inversion examples in this paper illustrated the accuracy of the map inversion algorithm, the efficiency of the process also deserves attention. Table 3 shows the efficiencies of map inversion relative to model inversion (i.e., solving the system of differential equations to acceptable accuracy for a single run). For the linear system, the map inversion was actually *less* efficient than model inversion because a simple analytic form for the model in eq 13 was available. Map evaluation was also less efficient than model evaluation for the HBr system, which is a small kinetic system involving few species. However, the HDMR algorithm outperformed model evaluation by more than a factor of 3 for the full inversion of the formaldehyde system and by a factor of almost 30 for the partial inversion of the formaldehyde system. Although there is an overhead associated with the sampling and construction of the HDMR maps, it is negligible compared to the cost of the inversion process. In general, systems with the most complicated, costly kinetic models will benefit the most from map inversion. In these cases, the model evaluation is prohibitively costly, and the inversion process can be greatly expedited by the use of a map generating algorithm such as HDMR.

IV. Conclusions

Data inversion to extract rate constants can benefit from increased computing power, but a sufficiently cost-intensive model often precludes thorough inversion using even the fastest computers. Methods such as conjugate gradient optimization, which limit the number of function evaluations, can be locally effective but neglect the possibility of globally distinct multiple solutions. The presence of multiple solutions can greatly influence rate constant uncertainties. To obtain a reliable and accurate understanding of rate constant uncertainties, a thorough yet efficient search of the parameter space must be performed. This process is made feasible by map inversion.

For the cases studied in this paper, map inversion proved to be an accurate technique for nonlinear model approximation. For the formaldehyde system, the speed of HDMR evaluation made possible an extensive exploration of the parameter space, which would have been excessively time-consuming using conventional methods. Monte Carlo error analysis was also facilitated by the maps. In general, any process that relies on repeated model evaluation can be expedited by the use of an appropriate map function.

More advanced map-facilitated inversion algorithms can be developed with HDMR and possibly other techniques.[23] In some cases, it may be more efficient to use a series of quasi-local nonlinear maps rather than seek a single global map. These general techniques hold promise for providing more thorough

and reliable inversions of laboratory data in chemical kinetics as well as other applications.

Acknowledgment. We acknowledge support from the Princeton Plasma Physics Laboratory and the Air Force Office of Scientific Research.

References and Notes

(1) Fahr, A.; Braun, W. *Int. J. Chem. Kinet.* **1994**, *26*, 535.
(2) Yetter, R. A.; Rabitz, H.; Dryer, F. L.; Maki, R. G.; Klemm, R. B. *J. Chem. Phys.* **1989**, *91* (7), 4088.
(3) Caralp, F.; Devolder, P.; Fittschen, C.; Gomez, N.; Hippler, H.; Méreau, R.; Rayez, M. T.; Stiebel, F.; Viskolcz, B. *Phys. Chem. Chem. Phys* **1999**, *1*, 2935.
(4) DeMore, W. B.; Bayes, K. *J. Phys. Chem. A* **1999**, *103*, 2649.
(5) Michael, J. V.; Kumaran, S. S.; Su, M.-C. *J. Phys. Chem. A* **1999**, *103*, 5942.
(6) Bard, Y. *Nonlinear Parameter Estimation*; Academic Press: New York, 1974.
(7) Lisý, J. M.; Símon, P. *Comput. Chem.* **1998**, *22* (6), 509.
(8) Farinha, J.; Martinho, J.; Pogliani, L. *J. Math. Chem.* **1997**, *21*, 131.
(9) Goldberg, D. E. *Genetic Algorithms in Search, Optimization, and Machine Learning*; Addison-Wesley: Reading, MA, 1989.
(10) Rabitz, H.; Aliş, Ömer F.; Shorter, J.; Shim, K. *Comput. Phys. Commun.* **1998**, *117*, 11.
(11) Vajda, S.; Rabitz, H. *J. Phys. Chem.* **1988**, *92*, 701.
(12) Vajda, S.; Rabitz, H. *Chem. Eng. Commun.* **1989**, *83*, 191.
(13) Alper, J. S.; Gelb, R. I. *J. Phys. Chem.* **1990**, *94*, 4747.
(14) Alper, J. S.; Gelb, R. I. *J. Phys. Chem.* **1991**, *95*, 104.
(15) Rabitz, H.; Shim, K. *J. Chem. Phys.* **1999**, *111*, 10640.
(16) Shorter, J. A.; Ip, P. C.; Rabitz, H. *J. Phys. Chem. A* **1999**, *103*, 7192.
(17) Bevington, P. R.; Robinson, D. K. *Data Reduction and Error Analysis for the Physical Sciences*; McGraw-Hill: New York, 1992.
(18) Hindmarsh, A. C. *Scientific Computing*; 1983, pp 55−64.
(19) Gear, C. W. *Numerical Initial Value Problems in Differential Equations*; Prentice Hall: Englewood Cliffs, NJ, 1970.
(20) Press, W. H.; Teukolsky, S. A.; Vetterling, W. T.; Flannery, B. P. *Numerical Recipes in C: The Art of Scientific Computing*, 2nd ed.; Cambridge University Press: Cambridge, U.K., 1993.
(21) Rabitz, H.; Aliş, Ö. F. *J. Math. Chem.* **1999**, *25*, 197.
(22) Rabitz, H.; Aliş, Ö. F. in *Sensitivity Analysis*; John Wiley and Sons: New York, 2000; pp 199−223.
(23) Geremia, J. M.; Rabitz, H.; Rosenthal, C. Manuscript in preparation.
(24) http://lancet.mit.edu/ga/, 2001.
(25) Rojnuckarin, A.; Floudas, C. A.; Rabitz, H.; Yetter, R. A. *J. Phys. Chem.* **1993**, *97*, 11689.
(26) Laidler, K. *Chemical Kinetics*, 3rd ed.; Harper and Row: New York, 1987.
(27) Bodenstein, M.; Lind, S. C. *Z. Phys. Chem.* **1907**, 168−192.
(28) Glassman, I. *Combustion*, 2nd ed.; Academic Press: New York, 1987.
(29) Moore, J. W.; Pearson, R. G. *Kinetics and Mechanism*, 3rd ed.; John Wiley and Sons: New York, 1981.
(30) Kerr, J., Ed. *CRC Handbook of Bimolecular and Termolecular Gas Reactions*; CRC Press: Boca Raton, FL, 1981.